INTERNATIONAL TABLES FOR CRYSTALLOGRAPHY

ISSN 1574-8707
it.iucr.org

Volume I, X-ray Absorption Spectroscopy and Related Techniques
ISBN: 978-1-119-43394-1

Chapter 3.42

Keywords: X-ray absorption spectroscopy; X-ray emission spectroscopy; energy calibration; powder diffraction; single-crystal diffraction.

Energy calibration for X-ray spectroscopy using powder and single-crystal standards

Chanh Q. Tran,[a] Christopher T. Chantler[b]* and Martin D. de Jonge[c]

[a]Department of Mathematical and Physical Sciences, La Trobe University, La Trobe, Victoria 3086, Australia, [b]School of Physics, University of Melbourne, Victoria 3010, Australia, and [c]Australian Synchrotron, ANSTO, Clayton, Australia. *Correspondence e-mail: chantler@unimelb.edu.au

Determination of energy and a calibrated energy scale are critical for most X-ray science. At X-ray absorption spectroscopy synchrotron beamlines, a single reference foil is often used to give a single-point transfer for energy at the active absorption *K* edge. Sometimes, more complex diagnostics are used. Yet, beamline or laboratory optics can result in numerous systematic errors with structure resulting from the heat load, monochromation, mechanical and thermal drift, harmonic rejection mirrors, orientation and offsets. This chapter focuses on the use of single-crystal X-ray diffraction and powder crystal X-ray diffraction standards for energy calibration across the energy range of the experiment, whether for X-ray absorption spectroscopy or X-ray diffraction.

1. Introduction

Crystallography depends upon the incident energy and bandwidth of the source. Very often the actual energy and the calibration of energy are secondary, as the structure of the unknown at whatever temperature, pressure, phase, crystallinity and form is more important for the science and significance. For example, measurements of pre-edge, edge and XANES structure are often dominated by small shifts, where high accuracy and stability of these small shifts are essential, but where energy shifts relative to known reference materials are often of the most interest and direct relevance, even though an absolute energy scale remains desired and of value. Similarly, the use of known references (reference foil characteristic edge determinations) is generally essential and often sufficient, although much of the literature does not have an absolute energy calibration of the edge positions. For EXAFS or XAFS spectra, it is increasingly important and valuable to use multipoint energy calibration since it has a direct bearing on the distance determinations. In general, a 1% error in the energy scale yields a 1% error in bond lengths or correlations with other, often free, parameters. Some software packages can fit absolute energies, but many fit energies or momenta k relative to the edge position, so errors in this can invalidate low-k analysis and yield significant distortions for, for example, a k of about 2–3 Å^{-1}.

Nonetheless, standards laboratories have spent many decades defining and marketing the use and implementation of single-crystal X-ray diffraction standards and powder X-ray diffraction standards, as are well presented in the second edition of Volume C of *International Tables for Crystallography*. Since the definition of the X-ray energy relative to the optical wavelength and frequency, in ångströms or in nanometres, in 1985, key standards laboratories in the USA, France, Germany, Australia and elsewhere have worked to make

Related chapters

Volume I: 3.4, 3.5, 3.6, 3.7, 3.11, 3.14, 3.38, 3.39, 3.43, 3.48, 4.2, 4.6

portable standards, especially for high-accuracy measurements where the energy should be calibrated to below 1 p.p.m., for example to below 0.01 eV for a 10 keV photon (Chantler *et al.*, 2024). An advantage of these standards is that they can be used across a continuous energy range and thus are not, for example, a single fixed-point energy measurement of a characteristic $K\alpha$ peak nor a specific absorption K-edge energy (Diaz-Moreno, 2012). Some groups (Acrivos *et al.*, 1982; Pettifer & Hermes, 1985; Stümpel *et al.*, 1991) have proposed the use of Laue diffraction or the Bond method to establish the energy scale; a comment has been that, unless set up for routine measurement, these setups can require considerable additional time (Diaz-Moreno, 2012).

In application to energy calibration at synchrotron beamlines, including for X-ray absorption spectroscopy (XAS), powder and single-crystal diffraction have been used to investigate or characterize optical transfer functions, offsets and linear calibration errors for the whole beamline. These experiments do not use the primary monochromator, as this is often too heavily impacted by the heat load (Barnea *et al.*, 1992; Chantler, Tran, Barnea *et al.*, 2001; Chantler *et al.*, 2004), and they do not usually use a secondary, cooled or coupled, monochromator plane. Instead, they use a crystal diffracting analyser near the sample to measure the bandwidth and energy distribution at the sample, including the whole optic, monochromator, mirrors, apertures, drifts, off-axis errors and other systematic errors. As such, we do not need to discuss here the changes in monochromator energy on tuning or detuning or the stability of the beam energy under heat load: the beam energy, distribution and stability should be measured.

Energy standards are often provided by single metal foils for a specific energy. For the current status of these approaches, for both characteristic energy determination and absorption-edge determination, see Chantler (2024*a*) and Chantler *et al.* (2024). For a set of data that are suitable for this purpose to a higher level, see Chantler (2024*b*). This relates to the general topic of calibration and diagnostics (Diaz-Moreno, 2024).

Backscattering (that is, the use of a near back-reflection from crystal diffraction using a perfect crystal analyser) is a subset of the class of direct methods to be discussed here. This is subject to alignment issues, including poor signal to noise, ambiguous identification of high Miller indices and ambiguity of azimuthal orientation; we are not aware of detailed studies or reports on this approach.

Bragg glitches in the monochromator crystal – that is, two-beam X-ray diffraction peak interference or multiple-beam diffraction interactions – can be used very well and effectively with a knowledge of the monochromator crystal alignment to calibrate and determine energy and can be characterized as part of a well organized synchrotron calibration (Sutter *et al.*, 2016). Conversely, Bragg glitches in the sample (diffraction from crystalline samples, for example silicon) can also be used to determine sample quality, crystallinity and alignment, and also to measure energy (Tran, Chantler *et al.*, 2003; Chantler *et al.*, 2010), although usually these are of lower quality for uncharacterized samples.

The dominant topic to discuss here is the use of single-crystal or powder diffraction standards to measure and calibrate the energy of the incident beam coming into or out of the sample. As reported in Volume C of *International Tables for Crystallography* (Parrish *et al.*, 1999), the best documented and most widely used standards for powder diffraction are those from the (US) National Institute of Standards and Technology (Dragoo, 1986) for Si 640 (Hubbard *et al.*, 1975), Si 640a (Hubbard, 1983), Si 640b (Wong-Ng & Hubbard, 1987), Si 640c (Freiman *et al.*, 2000*a*), LaB_6 660 and LaB_6 660a (Freiman *et al.*, 2000*b*). Other standards for energy include tungsten and silver, fluorophlogopite (mica) SRM 675 and the five intensity standards SRM 674 [α-Al_2O_3 (corundum), ZnO, TiO_2 (rutile), Cr_2O_3 and CeO_2]. This total is a sparse set (that is, there are few standards reported in the literature), especially for powder diffraction and energy standards; within this sparse set current availability is further limited to Si 640c and LaB_6 660a. Although Si 640c has the highest reported accuracy, it is also limited by the number of available reflections, especially at low X-ray energies; LaB_6 660a, with a lower reported accuracy, often has well placed and numerous diffraction peaks at these lower energies.

Powder diffraction standards have been used: the NIST powder standards Si 640b (Parrish *et al.*, 1999) and LaB_6 660 (Rasberry *et al.*, 1989) were used by Chantler, Tran, Paterson *et al.* (2001), Tran, Barnea *et al.* (2003), Glover *et al.* (2008, 2010) and Islam *et al.* (2014), the NIST powder standard Si 640b was used by Tran *et al.* (2005) and the NIST powder standards Si 640c and LaB_6 660a (Freiman *et al.*, 2000) were used by Islam *et al.* (2010), Tantau *et al.* (2015) and Sier *et al.* (2020). The approach has been detailed for powder measurements (Chantler *et al.*, 2004, 2007; Rae *et al.*, 2006; Tantau *et al.*, 2014). Over the energy range 5–20 keV, powder diffraction methods are well suited to energy determination and structural evaluation given appropriate techniques and standards (Chantler *et al.*, 2004).

Figs. 1 and 2 show the general features of an experimental arrangement for the calibration of energy-on-sample using powder diffraction. The examples described here are for the measurement of mass attenuation for copper metal from 8.85 to 20 keV, and for silicon from 5 to 20 keV, at the Australian National Beamline Facility (ANBF), Japan. At ANBF, the incident beam was monochromated by double reflection from a silicon monochromator, which could be detuned to minimize the harmonic components and optimize the throughput (Materlik & Kostroun, 1980). The monochromated beam was then collimated by a set of slits which defined the beam size to approximately 1×1 mm with a vertical divergence of 0.12 ± 0.03 mrad.

The collimating system was followed by the BigDiff powder diffractometer (Barnea *et al.*, 1989, 1992), in which the standard powder specimens Si NIST SRM 640b [a_0 = 5.430940 (11) Å] and LaB_6 NIST SRM 660 [a_0 = 4.15695 (6) Å] (Parrish *et al.*, 1999) were used (unsorted as to particle size) to determine the energy of the X-rays. Six or eight (20×40 cm) image plates of 100 µm (0.01° equivalent) resolution mounted in the diffractometer at 0.573 m radius covered an angular

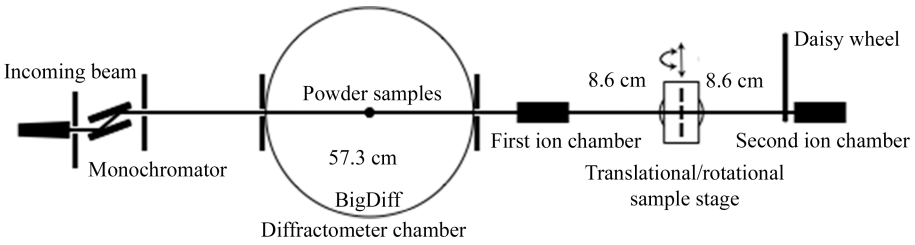

Figure 1
Example experimental layout for energy calibration using powder diffraction in precise measurement of the absorption coefficient of copper metal from 8.85 to 20 keV and of a silicon single crystal from 5 to 20 keV conducted in a single beamtime on ANBF beamline 20B, Photon Factory, Tsukuba, Japan (Chantler *et al.*, 2004). The radius of the diffractometer r = 57.3 cm. Nonlinearities and slopes with energy can be very significant even on short timescales.

range from −120° to 120° (Sabine *et al.*, 1995; Figs 2 and 3). The angular positions of these image plates were determined from the positions of a set of fiducial marks provided by radioactive sources embedded in the perimeter of the diffractometer.

With this bending-magnet second-generation source, powder diffraction patterns required exposures from a few minutes to approximately 30 min depending upon the energy and the diffraction-peak strengths and the powder transparency (Fig. 4). This setup was well designed and perfectly suitable, but was certainly not optimized for space or speed or for transferability into beamline-control systems. Much more could be performed, for example, with a powder on a four-circle goniometer (see below) and much faster. Some 10–20 measurements of energy are usually plenty to characterize the full calibration functional, even across an extended energy range. To establish an energy scale, effects from any deviation from ideal alignment of the diffractometer must be corrected for. These include offsets of the powder sample from the central axis of the diffractometer, offsets in the pre-calibrated positions of the image plates (detectors), the divergence and bandwidth of the incident beam and the absorption of the powder sample. In principle, one single measurement might determine a constant offset, two measurements might characterize a linear offset, three measurements would distinguish between an energy or slope offset and an angle offset or slope, and six measurements would overdetermine such simple systems and provide an error functional for uncertainty. Over more extended ranges, extra measurements might characterize other, observed, nonlinearities. In all cases, these sparse measurements, if well set up, can take just minutes.

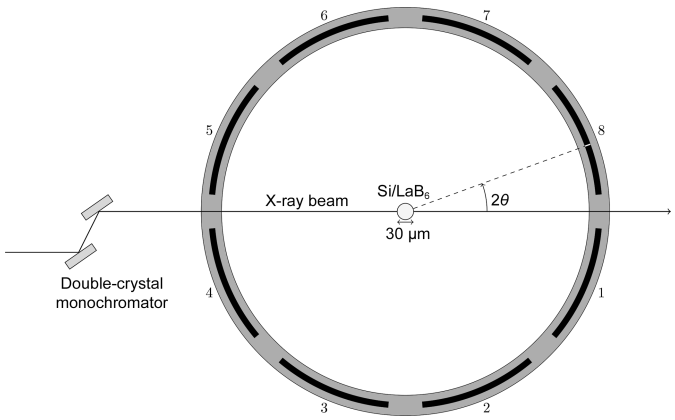

Figure 2
Schematic of the BigDiff powder diffractometer (Barnea *et al.*, 1989; Chantler *et al.*, 2004). The locations of the eight image plates are represented as thick black lines surrounding the rim of the chamber. Details are given in the text.

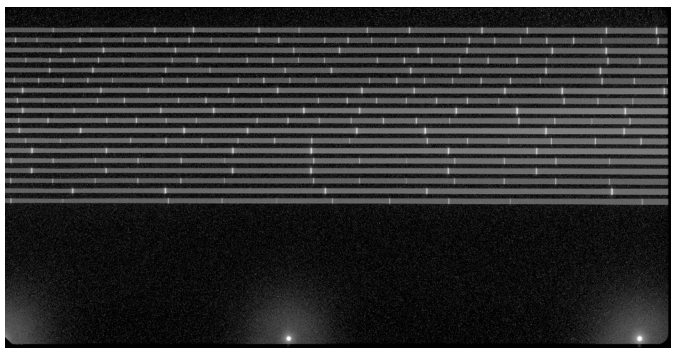

Figure 3
A typical image plate, which in this case spanned from −45° to −86°. 18 different powder diffraction patterns were taken, with each producing one of the horizontal stripes, within which thin vertical stripes corresponding to diffraction peaks are present. The two bright spots at the bottom of the plate are the radioactive fiducial markers.

2. Energy analysis: consistency of powder diffraction energy determinations and (re-)calibration of synchrotron beamline monochromation

In the illustrated experimental setup at ANBF, each image plate k must be corrected for a constant offset of the recorded angular 2θ positions $\delta\theta_k$ (in other words, a slight misalignment of the radioactive fiducials used to determine the plate locations) of up to 0.04° or 400 μm, equivalent to approximately 10–30 eV. These corrections are consistent for the set of all (say 10–20) exposures taken at different energies with the same image plate, as expected. A linear fitting model was therefore applied using a constant offset in the angular positions of the powder lines for each image plate to locate the predefined positions of the radioactive fiducials on an absolute scale. In other words, $\theta = \theta_{\rm meas} + \delta\theta_k$. As a consequence, the defining equation for diffraction peak $(hkl)_j$ for energy E_i, where a_0 is the lattice parameter, can be written as

Table 1
Example energy calibration using Si 640b and LaB_6 powder standards for the energies used with copper attenuation samples following Chantler *et al.* (2004).

Data are presented in order of measurement. The nominal energies (E_{nom}) at which the calibrations were conducted are compared with the calibrated energies using Si 640b (E_{Si}) and LaB_6 (E_{LaB_6}). $\sigma_{E_{Si}}$ and $\sigma_{E_{LaB_6}}$ are the one standard error uncertainties corresponding to E_{Si} and E_{LaB_6}, respectively. $E_{LaB_6} - E_{Si}$ is the difference in electronvolts between the determined energies, with the corresponding σ given. The calibrated energies using the Si 640b and LaB_6 660 powder standards, which are consistent within 1 eV, reveal the possibility of high-accuracy measurement using powder standards.

E_{nom} (keV)	E_{Si} (keV)	$\sigma_{E_{Si}}$ (eV)	E_{LaB_6} (keV)	$\sigma_{E_{LaB_6}}$ (eV)	$E_{LaB_6} - E_{Si}$ (eV)	$\sigma_{E_{LaB6}-E_{Si}}$ (eV)
20.0	20.0279	0.55	20.0296	0.62	1.70	0.83
18.6	18.7043	0.61	18.7060	0.47	1.70	0.78
17.6	17.6959	0.59	17.6972	0.51	1.30	0.78
15.6	15.6762	0.36	15.6776	0.39	1.40	0.53
14.0	14.0638	0.40	14.0659	0.30	2.10	0.50
13.0	13.0575	0.45	13.0588	0.26	1.30	0.52
12.0	12.0500	0.37	12.0515	0.26	1.50	0.45
11.0	11.0429	0.39	11.0433	0.16	0.40	0.42
10.0	10.0386	1.23	10.0361	0.19	−2.50	1.25
9.10	9.1322	0.40	9.1328	0.35	0.59	0.53
8.95	8.9817	0.38	8.9828	0.35	1.12	0.51

$$\theta_{meas} = \arcsin\left[\frac{hc}{2d_j E_i}\right] - \delta\theta_k, \tag{1}$$

where

$$d_j = \frac{a_0}{(h_j^2 + k_j^2 + l_j^2)^{1/2}}$$

is the lattice spacing.

This equation can be linearized to give a more convenient form for least-squares fitting,

$$\sin\theta_{i,j} \simeq \sin\theta_{meas,j} + \delta\theta_k \cos\theta_{meas,j}. \tag{2}$$

Substituting $hc/2d_jE_i = \sin\theta_{i,j}$ into equation (2) and moving the lattice spacing, d_j, to the right-hand side yields

$$\frac{hc}{2E_i} \simeq d_j \sin\theta_{meas,j} + \delta\theta_k d_j \cos\theta_{meas,j}. \tag{3}$$

At each energy E_i, equation (3) can be used to fit for E_i $\delta\theta_k$ using the measured angular positions $\theta_{means,j}$ and the corresponding lattice spacings d_j.

The eccentricity of the powder sample from the centre of the diffraction chamber is characterized by a vertical offset δ_y and a horizontal offset δ_z. For small displacements the corresponding angular shifts are

$$\delta\theta_y \simeq \frac{\delta_y}{D\cos 2\theta}, \quad \delta\theta_z \simeq \frac{\delta_z}{D\sin 2\theta}, \tag{4}$$

where D is the diameter of the diffraction chamber. These forms of δ_y and δ_z orthogonalize the components and minimize correlations between the two parameters. The offsets of the powder sample, δ_y and δ_z, can be incorporated into the fitting of the incident energy by substituting $\delta\theta_k$ by $[\delta\theta_k + (\delta_y/D\cos 2\theta) + (\delta_z/D\sin 2\theta)]$,

$$\arcsin\left(\frac{hc}{2dE}\right)\theta + \delta\theta_k + \frac{\delta_y}{D\cos 2\theta} + \frac{\delta_z}{D\sin 2\theta}. \tag{5}$$

The results for energy determinations using the Si 640b and LaB_6 660 powder standards in the measurement of the mass attenuation coefficient of copper are shown in Table 1. The fitted uncertainties matched the variation observed between fits, indicating that the computation was robust and self-consistent. These are simply typical accuracies and uncertainties from this method using a bending-magnet second-generation flux beamline. In principle, a well optimized experimental setup could return this quality and better within minutes.

The results for energy determination over 16 energies using the Si 640b and LaB_6 660 powder standards in measurement of the mass attenuation coefficient of silicon are summarized and compared in Table 2.

Separate fits of individual image plates were used to assess the self-consistency of local results with the final averages and to identify any possible outliers. Insignificant differences were obtained compared with the fits of all plates in Table 1. The resultant energies obtained with the two powder standards were averaged with the weighting derived from the corresponding errors.

Energies from both powder determinations were highly consistent. Best-fit linear or quadratic interpolated energy calibrations on piecewise-continuous regions yield very a high accuracy of transfer of standards. The energy calibration in the silicon experiment determined corrections to the nominal,

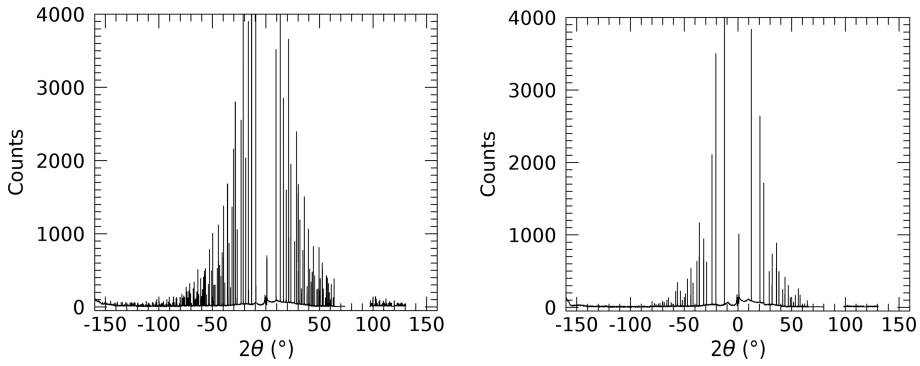

Figure 4
Extracted powder diffraction patterns for lanthanum hexaboride (LaB_6; left) and silicon (right) at a nominal energy of 15 keV.

Table 2
Example energy calibration using Si 640b and LaB_6 powder standards for energies from silicon attenuation measurement (Chantler *et al.*, 2004).

Data are presented in order of measurement. The nominal energies (E_{nom}) at which the calibrations were conducted are compared with the calibrated energies using Si 640b (E_{Si}) and LaB_6 (E_{LaB_6}). $\sigma_{E_{Si}}$ and $\sigma_{E_{LaB_6}}$ are the one standard error uncertainties corresponding to E_{Si} and E_{LaB_6}, respectively. The calibrated energies using the Si 640b and LaB_6 660 powder standards, which are consistent within 1 eV, reveal the possibility of high-accuracy measurement using powder standards and of powder standards.

E_{nom} (keV)	E_{Si} (keV)	$\sigma_{E_{Si}}$ (eV)	E_{LaB_6} (keV)	$\sigma_{E_{LaB_6}}$ (eV)	$E_{LaB_6} - E_{Si}$ (eV)	$\sigma_{E_{LaB6}-E_{Si}}$ (eV)
5.0			5.0146	1.08		
6.0	6.0106	0.57	6.0112	1.56	0.62	1.66
7.0	7.0111	1.56	7.0110	0.90	−0.09	1.80
7.4	7.4139	0.15	7.4138	0.95	−0.01	0.96
7.6	7.6130		7.6131	0.32	0.06	0.32
8.0	8.0135	0.28	8.0136	1.10	0.10	1.13
9.0	9.0135	0.28	9.0156	1.09	2.17	1.13
9.0	9.0143	0.96	9.0168	0.89	2.50	1.30
10.0	10.0171	0.65	10.0175	0.89	0.41	1.10
11.0	11.0207	0.87	11.0205	0.82	−0.23	1.20
12.0	12.0205	0.90	12.0215	0.99	1.03	1.34
13.5	13.5214	0.90	13.5216	0.90	0.28	1.27
15.0	15.0228	0.71	15.0236	0.82	0.81	1.08
16.2	16.2251	0.47	16.2258	1.04	0.72	1.14
17.6	17.6266	1.20	17.6294	0.95	2.82	1.53
18.6	18.6269	0.65	18.6273	0.54	0.39	0.85
20.0	20.0278	1.39	20.0285	0.81	0.64	1.61

pre-calibrated, energy of the monochromator of 10–30 eV (Table 2; Tran, Barnea *et al.*, 2003; Chantler *et al.*, 2004). Interestingly, these corrections in the copper experiment were 20–110 eV (Table 1; Chantler, Tran, Paterson *et al.*, 2001; Chantler *et al.*, 2004). The differences in corrections are due to hysteresis of the monochromator: for the copper measurements the data were acquired in order of decreasing energy, while for silicon the data were acquired with increasing energy. Perhaps surprisingly, these corrections were quite large (Fig. 5)! For each well determined energy (for example 10 keV) in each experiment, the determinations corresponded to a mean $|\Delta\theta| = 0.00040$–0.00048° for some 17–77 measured peaks.

The uncertainty of these corrected energy values, σ, varied from 0.34 to 2.4 eV in the silicon experiment, corresponding to energy determinations from 28 to 350 p.p.m. The copper experiment determined weighted mean energies with one standard deviation σ from 0.14 to 1.0 eV, corresponding to energy determinations from 13 to 72 p.p.m.

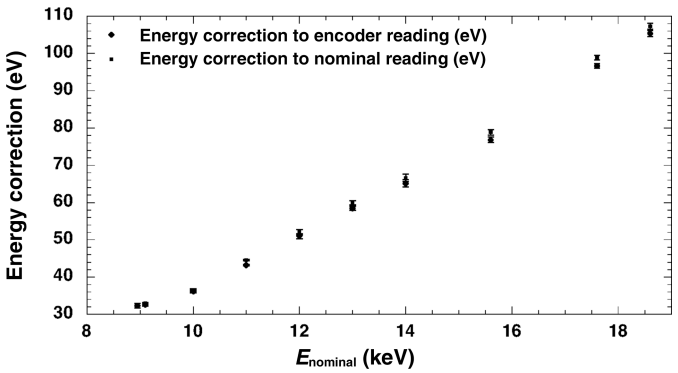

Figure 5
Energy correction from the copper experiment derived from the weighted mean of the silicon and LaB_6 powder standard determinations applied to nominal monochromator energy and nominal calibrated encoder energies, respectively, following Chantler *et al.* (2004).

The resulting accuracies were limited at low energies by air attenuation, resulting in few and weak peaks on each imaging plate, and at higher energies by the difficulty of uniquely determining the indices of many closely spaced and weak peaks at very high angles. In both cases these are reflected in the uncertainty estimates.

Whilst relative energy measurements to within about 1 eV have often been achieved, absolute energy determinations remained uncertain to about 10 eV in a variety of past experiments, particularly if detuning was used to monochromate the beam, if the beam was off-axis, if the monochromator drifted or if direct recalibrations were not performed. The use of powder standards is able to accurately calibrate synchrotron beamline monochromation in the presence of detuning shifts or mechanical hysteresis. This can also be used to calibrate secondary powder lattice standards (Chantler *et al.*, 2004, 2007; Rae *et al.*, 2006) and can be used to recalibrate edge-energy determinations, which are often used as a primary or secondary standard (Chantler *et al.*, 2004; Tantau *et al.*, 2014).

3. Ability of energy measurement to measure secondary beam characteristics on the sample: beam divergence and bandwidth

The widths of the powder diffraction peaks can be investigated to confirm their consistency with the image-plate resolution, capillary dimension, powder transparency, and beam divergence and bandwidth (Chantler *et al.*, 2004; Bunker, 2023). Widths varied from close to the image-plate resolution limit of 0.01° (Cookson, 1998) to typically 0.07° or so, particularly for the lowest order, strongest reflection or for the highest angle reflections (Chantler, Tran, Barnea *et al.*, 2001; Tran, Chantler *et al.*, 2003; Chantler *et al.*, 2004). Fitting precision for widths was generally good and varied from extremes of $\sim 0.00001^\circ$ to $\sim 0.01^\circ$ after allowance for $(\chi^2_r)^{1/2}$. Typical uncertainties in angle were 0.0001–0.001°.

The logic and functional form of the observed widths can also be investigated (Chantler *et al.*, 2004). The vertical divergence of the X-ray beam results in a broadening of the powder diffraction lines, similar to the broadening δ_E due to the energy window ΔE. The observed linewidths of the diffraction peaks depend on contributions from several factors: the divergence of the incident beam δ_{div}, the energy window of the incident beam ΔE, the linewidth of the rocking curve of the powder sample δ_s, the size of the powder sample δ_{sz}, the absorption of the powder sample, and the detector resolution δ_{det}. The beam divergence δ_{div} depends on the geometry of the experimental arrangement, and in our energy measurement the vertical component of the beam divergence appears to dominates over the horizontal component, noting that the measurement is substantially more sensitive to the vertical component. To first order, in a Gaussian approximation, all of the factors mentioned above are independent of

each other and the observed linewidths add these contributions in quadrature,

$$\delta\theta^2_{\rm meas} = \delta^2_{\rm sz} + \delta^2_{\rm div} + \delta^2_{\rm det} + \delta_E(\theta)^2 + \delta_{\rm s}(\theta)^2. \quad (6)$$

However, the first three terms are of the same order: $\delta_{\rm sz} \simeq [\tan^{-1}(0.1\ {\rm mm}/R)] \simeq 0.01^\circ$, $\delta_{\rm div} \simeq 0.007^\circ$ and $\delta_{\rm det} \simeq 0.01^\circ$. $\delta_E(\theta)$ and $\delta_{\rm s}(\theta)$ have significant dependencies upon θ and E. $\delta_{\rm s}(\theta)$ can contribute to the lowest order reflection(s), where the diffraction width might reach 0.004° or more, but for higher order reflections the diffraction width, as opposed to the geometrical broadening, is usually negligible at only a few arcseconds. From Bragg's law, we have

$$\delta_E(\theta) = \frac{\Delta E}{E}\tan\theta. \quad (7)$$

The broadening due to the bandpass $\delta_E(\theta)$ becomes significantly larger with angle and rapidly dominates over all of the other contributions. Therefore, if we plot $\delta\theta^2_{\rm obs}$ as a function of $\tan^2\theta$ then the energy bandpass of the monochromated incident beam can be obtained from the slope of the plot. Note that in powder research a different dependence of full width at half maximum is often cited (Freiman *et al.*, 2000) of the form

$$\delta\theta_{\rm obs} = A/\cos\theta + B\tan\theta, \quad (8)$$

where A and B are interpreted to relate to crystal size and microstrain, respectively. This is not a unique physical interpretation, implying that the parameters derived from such an investigation may have little physical meaning. Further, this form does not appear to match the data of Chantler *et al.* (2004). Therefore, either these effects are absent in this case or the physical model is inappropriate.

The y intercept of the plot of $\delta\theta^2_{\rm obs}$ versus $\tan^2\theta$ includes the intrinsic divergence of the beam $\delta_{\rm div}$, the source size $\delta_{\rm sz}$ and the detector resolution $\delta_{\rm det}$.

The profile shapes are important and, because of this, in general the convolved linewidth δ_{y0} is significantly less than the quadrature sum,

$$\delta\theta^2_{\rm obs} \simeq \delta^2_{y0} + \delta_E(\theta)^2 + \delta_{\rm s}(\theta)^2,$$
$$\delta^2_{y0} \ll \delta^2_{\rm sz} + \delta^2_{\rm div} + \delta^2_{\rm det},$$
$$\delta^2_{y0} > \max(\delta^2_{\rm sz}, \delta^2_{\rm div}, \delta^2_{\rm det}). \quad (9)$$

Fig. 6 shows a typical plot at 10 keV. This shows the general consistency of the dependence of the profile width upon angle. A small discrepancy at low diffraction angles is a result of a small misalignment of the system.

The relative energy bandpass $\Delta E/E$ increases with energy (Fig. 7). This increase follows Bragg's law applied to quantify the energy bandpass of the monochromator for a particular lattice plane,

$$\Delta E/E = \delta d_{\rm mono}/d_{\rm mono} + \cot\theta_{\rm mono}\delta\theta_{\rm mono}. \quad (10)$$

At higher energies, the Bragg angles at the monochromator $\theta_{\rm mono}$ decrease, leading to an increase in the energy window of the incident beam $\Delta E/E$. The linewidths were consistent with a convolution of widths due to the vertical divergence, the monochromator bandpass, the sample width in the beam and the image-plate reader resolution. The clarity of these physical trends indicates both the quality and the consistency of the data.

This in turn allowed determination of the energy bandwidth or the degree of monochromaticity of the X-ray beam. Final estimates from experimental energy bandwidths varied between 1.6 eV (full width at half maximum) and almost 9 eV for the highest 20 keV energies (Chantler *et al.*, 2004).

4. Single-crystal diffraction energy measurement for XAS: an example

Single-crystal diffraction has been used (de Jonge, 2005; de Jonge *et al.*, 2005, 2007), using a germanium single crystal and especially the {*hhh*} manifold: h = 1–17. High-accuracy low-stress silicon and germanium monochromator-standard single crystals are excellent candidates for calibration and energy measurement. In principle, the whole crystallographic database of single-crystal structures allows many possible reference lattice materials, although few can compete with the quality of silicon and germanium in the central X-ray regime.

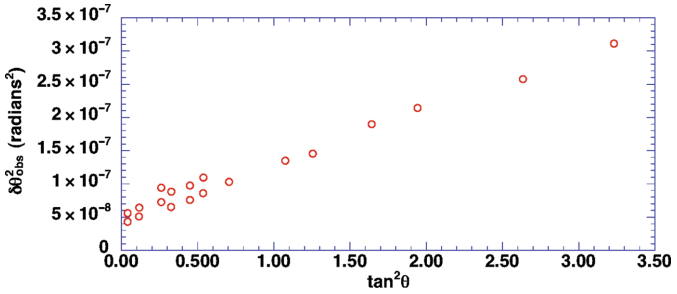

Figure 6
Linear dependence of $\delta\theta^2_{\rm obs}$ versus $\tan^2\theta$ for a synchrotron beam energy of 10 keV (equations 6 and 7), following Chantler *et al.* (2004). The slope represents the energy window $\Delta E/E$ and the y intercept gives the convolved width of the beam divergence, source size and detector resolution: in this case, approximately 0.02°. Error bars are approximately the size of the circles.

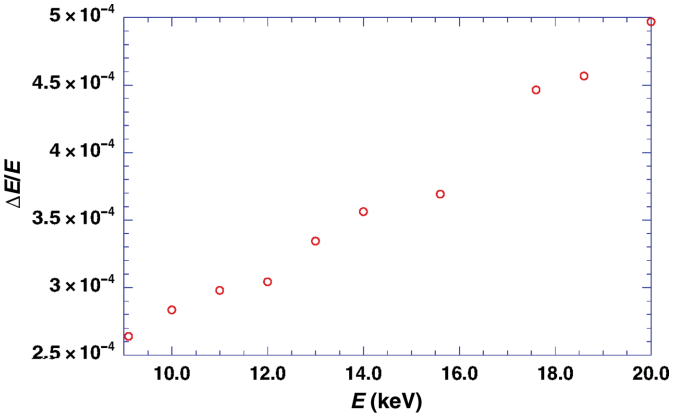

Figure 7
Energy bandpass $\Delta E/E$ versus energy E. The increase in $\Delta E/E$ as a function of energy E is in agreement with the prediction of equation (10).

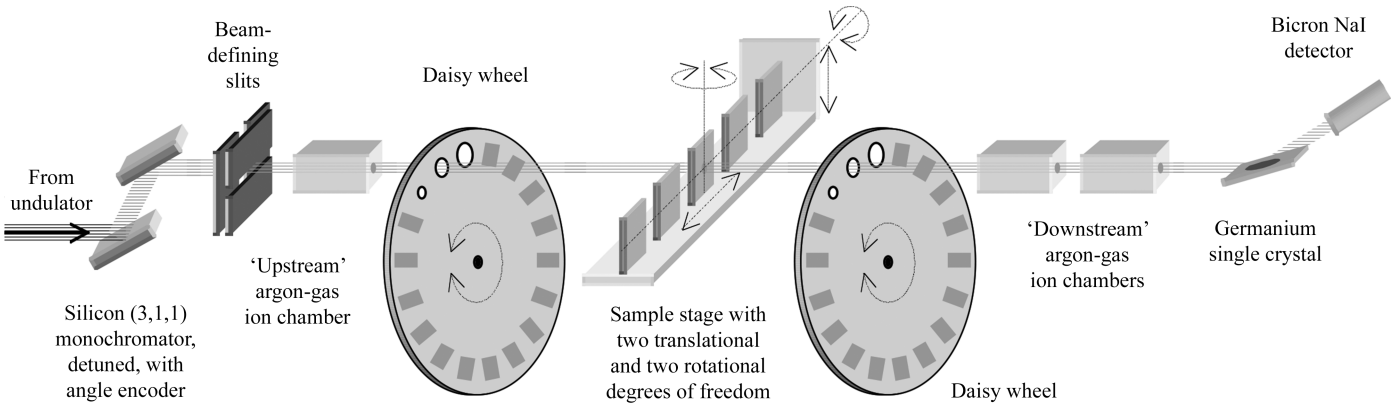

Figure 8
Schematic of the experimental layout for single-crystal diffraction energy calibration in an experiment for the precise measurement of X-ray absorption spectroscopy and mass attenuation coefficients of molybdenum (de Jonge *et al.*, 2005).

The photon energy was directly determined by diffraction from a germanium crystal mounted on a Huber four-circle diffractometer (Fig. 8). Foils mounted on the daisy wheel were introduced into the beam path to optimize the intensity of the X-ray beam used to measure the rocking curves.

Rocking curves were recorded with the X-ray intensity diffracted into a stationary sodium iodide scintillation detector whose face was centred on the predicted Bragg angle. The detector used was 'wide open', with no further angular selection applied to the diffracted beam. The germanium crystal was rotated through a small range of angles about the Bragg angle to record the rocking curve of the diffraction peak. Between 3 and 13 such rocking curves were recorded at each directly measured energy, diffracted by lattice planes {*hhh*} with h ranging from 1 to 17. The angular locations of these rocking curves were determined by fitting with a Lorentzian and also by determining their centres of mass. Two independent techniques for determining the angular locations were employed to avoid the effects of saturation of the detector used to measure the diffracted intensities (de Jonge, 2005).

The largest single source of systematic error in the energy determined in this manner is due to misalignment of the zero-angle position of the germanium crystal. We have corrected for this source of error using the same method as for powder calibration, presented in equations (1)–(3). Specifically, extrapolation of a plot of $d_{hkl}\sin\theta_{\mathrm{meas},hkl}$ versus $d_{hkl}\cos\theta_{\mathrm{meas},hkl}$ to the limit $\cos\theta_{hkl} = 0$ allows one to determine the energy of the beam from the $\sin\theta_{hkl}$ intercept, as well as the magnitude of the zero-angle misalignment of the germanium crystal. The lattice parameter of germanium used was a_0 = 5.65782 Å (Deslattes *et al.*, 1980).

Fig. 9 shows the results of this process, where the abscissa is the nominal synchrotron X-ray energy and the ordinate is the difference between the calibrated and nominal energies. The error bars represent the directly determined energies and the solid lines are the best fits to these energies determined using equation (11). The light grey lines above and below the fitted energies are the error estimates evaluated from the covariant error matrix returned from the fitting procedure. Using this procedure, the X-ray energies have been determined to a precision of between 0.0015% and 0.007% across the entire measurement range (de Jonge *et al.*, 2005). The monochromator angles were fitted separately over two energy ranges corresponding to the change from the fifth to the third undulator harmonic at about 25 keV, possibly resulting in a change in the value of the lattice parameter δ_{a_0} due to the different heat load.

The determined energies, depicted as points with error bars in Fig. 9, were used to calibrate the X-ray energy across the entire measurement range. This was achieved by fitting a modified Bragg function which related the monochromator angle, lattice parameter (Si) and Bragg planes ([3,1,1] family)

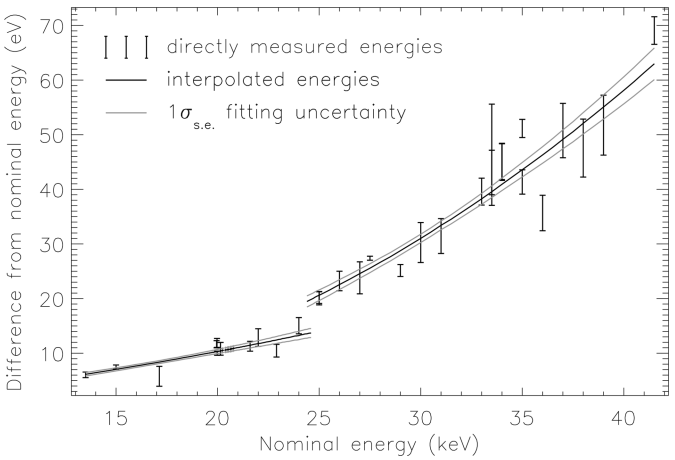

Figure 9
Results of the energy calibration following de Jonge *et al.* (2005). At several energies throughout the extended range, a series of {*hhh*} peaks were measured. These were used to determine the individual X-ray energies, represented here by the error bars. These energies were fitted to the monochromator crystal angle by equation (11) and this fitted function was used to interpolate the X-ray energy from the monochromator angle for the extended-range technique. The results of this fitting process and the interpolation are shown here by the line of best fit (black line) and the uncertainty (grey lines) estimated from the covariant error matrix returned by the fitting program.

to the directly determined energies. The fitting function used was

$$E = \frac{hc}{2d_{hkl}(1+\delta_{a_0})\sin(\theta+\delta_\theta)}, \quad (11)$$

which follows directly from Bragg's law, with a small adjustment to the monochromator lattice parameter via the parameter δ_{a_0}, allowing for expansion of the crystal due to the X-ray heat load, and an offset angle δ_θ of the monochromator crystal, which allows for mechanical slack in the crystal rotation stage and errors in the crystal alignment.

5. Discussion

For the examples presented here, the accuracy of energy determination is similar for single-crystal or powder methods because the dominant systematics arise from experimental resolution and fitting rather than from reference accuracy and uncertainty. We have selected examples here where the energy recalibration is strikingly large and very clearly essential. This is made more obvious by the large range measured in the experiments. For pre-edge measurement or some XANES, the offset between a set of measurements is particularly important, so beam optic stability is particularly important. The change of scale is quite hard to see or quantify. In many other cases, it may still be of the order of several electronvolts and important to investigate, whether as a routine operation or as a beamline characterization. Using a reference foil measurement can be useful to define a relative position to ~0.5–1.0 eV, but multipoint calibration is important for extended measurement and especially to define a calibration of structure and radial distances. For an ideal beamline, with no heat load, hysteresis, mirror focusing, alignment issues or changes with time, these measurements could be intermittent and periodic. For beamlines where the tuning or experimental setup changes with important process variables, these could be more important as routine components of the experiment.

The directly determined energies of these examples (copper, silicon and molydenum) are generally consistent with the smoothly interpolated fit, with a few points indicating a possible additional small variation of the beam energy that is not correlated with the monochromator angle. We commend the smoothly interpolated values in the final results, especially because the energy measurements are sparse. This could involve piecewise-continuous linear or quadratic interpolation or fits. The accuracy of the energy determination can be assessed by comparing the derived absorption-edge energy against the most accurate literature value.

The single-crystal method can be completed within minutes per energy to high accuracy, especially using a third-generation beamline, where it can be faster and more accurate. The method is relatively easy to implement using a six-circle goniometer.

6. Conclusion

For intermediate X-ray energy ranges, calibration of the energy at or near the sample is important and a check on any monochromation, mirror, mechanical or thermal offset or drift, or other optic functional on the delivered energy and bandpass at the experiment, is valuable. The use of a single edge energy with a little-known time-dependent bandwidth and resolution function to compare with a reference value does not measure the monochromator energy function across the energy range of the XAS scan. The use of powder and single-crystal standards provides the highest accuracy possible within the current standards and can be convenient and efficient if implemented routinely by beamline staff. It does require some space for suitable equipment. A regular monitor and check on energy, especially given the functionals of harmonic detuning and various operational implementations of this, and the variable energy functional and alignment of total-reflection harmonic rejection mirrors, encourages us towards a more reliable and controllable baseline, especially compared with a single *K*-edge offset reference with variable resolution. The selection of possible implementations presented here can be implemented at most XAS beamlines.

References

Acrivos, J. V., Hathaway, K., Reynolds, J., Code, J., Parkin, S., Klein, M. P., Thompson, A. & Goodin, D. (1982). *Rev. Sci. Instrum.* **53**, 575–581.

Barnea, Z., Clapp, R., Creagh, D. C., Sabine, T. M., Stevenson, A. W., White, J. W., Wilkins, S. W., Harada, J., Hashizume, H., Kashihara, Y., Sakata, M., Ohsumi, K. & Zemb, T. (1989). *Rev. Sci. Instrum.* **60**, 2537–2540.

Barnea, Z., Creagh, D. C., Davis, T. J., Garrett, R. F., Janky, S., Stevenson, A. W. & Wilkins, S. W. (1992). *Rev. Sci. Instrum.* **63**, 1069–1072.

Bunker, G. (2024). *Int. Tables Crystallogr. I*, ch. 3.45, 567–571.

Chantler, C. T. (2024*a*). *Int. Tables Crystallogr. I*, ch. 5.12, 687–689.

Chantler, C. T. (2024*b*). *Int. Tables Crystallogr. I*, ch. 7.4, 867–925.

Chantler, C. T., Rae, N. A. & Tran, C. Q. (2007). *J. Appl. Cryst.* **40**, 232–240.

Chantler, C. T., Smale, L. F. & Hudson, L. T. (2024). *Int. Tables Crystallogr. C*. In the press.

Chantler, C. T., Tran, C. Q. & Barnea, Z. (2010). *J. Appl. Cryst.* **43**, 64–69.

Chantler, C. T., Tran, C. Q., Barnea, Z., Paterson, D., Cookson, D. J. & Balaic, D. X. (2001). *Phys. Rev. A*, **64**, 062506.

Chantler, C. T., Tran, C. Q. & Cookson, D. J. (2004). *Phys. Rev. A*, **69**, 042101.

Chantler, C. T., Tran, C. Q., Paterson, D., Cookson, D. & Barnea, Z. (2001). *Phys. Lett. A*, **286**, 338–346.

Cookson, D. J. (1998). *J. Synchrotron Rad.* **5**, 1375–1382.

de Jonge, M. D. (2005). PhD thesis. University of Melbourne, Australia.

de Jonge, M. D., Tran, C. Q., Chantler, C. T., Barnea, Z., Dhal, B. B., Paterson, D., Kanter, E. P., Southworth, S. H., Young, L., Beno, M. A., Linton, J. A. & Jennings, G. (2007). *Phys. Rev. A*, **75**, 1–16.

de Jonge, M. D., Tran, C. Q., Chantler, C. T., Barnea, Z., Dhal, B. B., Cookson, D. J., Lee, W. & Mashayekhi, A. (2005). *Phys. Rev. A*, **71**, 032702.

Deslattes, R. D., Kessler, E. G., Sauder, W. C. & Henins, A. (1980). *Ann. Phys.* **129**, 378–434.

Diaz-Moreno, S. (2012). *J. Synchrotron Rad.* **19**, 863–868.

Diaz-Moreno, S. (2024). *Int. Tables Crystallogr. I*, ch. 3.48, 581–585.

Dragoo, A. L. (1986). *Powder Diffr.* **1**, 294–298.

Freiman, S. W., Trahey, N. M., Cline, J. P., Deslattes, R. D., Staudenmann, J., Kessler, E. G., Hudson, L. T., Henins, A., Cheary, R. W. & Filiben, J. J. (2000). *National Institute of Standards and*

Metrology SRM Certificates, Standard Reference Material 640c. https://tsapps.nist.gov/srmext/certificates/archives/640c.pdf.
Freiman, S. W., Trahey, N. M., Cline, J. P., Deslattes, R. D., Staudenmann, J., Kessler, E. G., Hudson, L. T., Henins, A., Cheary, R. W. & Filiben, J. J. (2000). *National Institute of Standards and Metrology SRM Certificates, Standard Reference Material 660a*. https://tsapps.nist.gov/srmext/certificates/archives/660a.pdf.
Glover, J. L., Chantler, C. T., Barnea, Z., Rae, N. A. & Tran, C. Q. (2010). *J. Phys. B At. Mol. Opt. Phys.* **43**, 085001.
Glover, J. L., Chantler, C. T., Barnea, Z., Rae, N. A., Tran, C. Q., Creagh, D. C., Paterson, D. & Dhal, B. B. (2008). *Phys. Rev. A*, **78**, 052902.
Hubbard, C. R. (1983). *Adv. X-ray Anal.* **26**, 45–51.
Hubbard, C. R., Swanson, H. E. & Mauer, F. A. (1975). *J. Appl. Cryst.* **8**, 45–48.
Islam, M. T., Rae, N. A., Glover, J. L., Barnea, Z., de Jonge, M. D., Tran, C. Q., Wang, J. & Chantler, C. T. (2010). *Phys. Rev. A*, **81**, 022903.
Islam, M. T., Tantau, L. J., Rae, N. A., Barnea, Z., Tran, C. Q. & Chantler, C. T. (2014). *J. Synchrotron Rad.* **21**, 413–423.
Materlik, G. & Kostroun, V. O. (1980). *Rev. Sci. Instrum.* **51**, 86–94.
Parrish, E., Wilson, A. J. C. & Langford, J. I. (1999). *International Tables for Crystallography*, Vol. C, edited by A. J. C. Wilson & E. Prince, ch. 5.2.10. Dordrecht: Kluwer Academic Publishers.
Pettifer, R. F. & Hermes, C. (1985). *J. Appl. Cryst.* **18**, 404–412.
Rae, N. A., Chantler, C. T., Tran, C. Q. & Barnea, Z. (2006). *Radiat. Phys. Chem.* **75**, 2063–2066.
Rasberry, S. D., Hubbard, C. R., Zhang, Y. & McKenzie, R. L. (1989). *National Institute of Standards and Metrology SRM Certificates, Standard Reference Material 660*. https://tsapps.nist.gov/srmext/certificates/archives/660.pdf.
Sabine, T. M., Kennedy, B. J., Garrett, R. F., Foran, G. J. & Cookson, D. J. (1995). *J. Appl. Cryst.* **28**, 513–517.
Sier, D., Cousland, G. P., Trevorah, R. M., Ekanayake, R. S. K., Tran, C. Q., Hester, J. R. & Chantler, C. T. (2020). *J. Synchrotron Rad.* **27**, 1262–1277.
Stümpel, J., Becker, P., Joksch, S., Frahm, R. & Materlik, G. (1991). *Phys. Status Solidi A*, **124**, 565–570.
Sutter, J. P., Boada, R., Bowron, D. T., Stepanov, S. A. & Díaz-Moreno, S. (2016). *J. Appl. Cryst.* **49**, 1209–1222.
Tantau, L. J., Chantler, C. T., Bourke, J. D., Islam, M. T., Payne, A. T., Rae, N. A. & Tran, C. Q. (2015). *J. Phys. Condens. Matter*, **27**, 266301.
Tantau, L. J., Islam, M. T., Payne, A. T., Tran, C. Q., Cheah, M. H., Best, S. P. & Chantler, C. T. (2014). *Radiat. Phys. Chem.* **95**, 73–77.
Tran, C. Q., Barnea, Z., de Jonge, M. D., Dhal, B. B., Paterson, D., Cookson, D. J. & Chantler, C. T. (2003). *X-ray Spectrom.* **32**, 69–74.
Tran, C. Q., Chantler, C. T., Barnea, Z., Jonge, M. D., Dhal, B. B., Chung, C. T. Y., Paterson, D. & Wang, J. (2005). *J. Phys. B At. Mol. Opt. Phys.* **38**, 89–107.
Tran, C. Q., Chantler, C. T., Barnea, Z., Paterson, D. & Cookson, D. J. (2003). *Phys. Rev. A*, **67**, 042716.
Wong-Ng, W. & Hubbard, C. R. (1987). *Powder Diffr.* **2**, 242–248.